Proteasome dysfunction induces excessive proteome instability and loss of mitostasis that can be mitigated by enhancing mitochondrial fusion or autophagy

Eleni N. Tsakiri, Sentiljana Gumeni, Konstantinos Vougas, Diana Pendin, Issidora Papassideri, Andrea Daga, Vassilis Gorgoulis, Gábor Juhász, Luca Scorrano and Ioannis P. Trougakos

Supplemental Information

Supplemental Figures

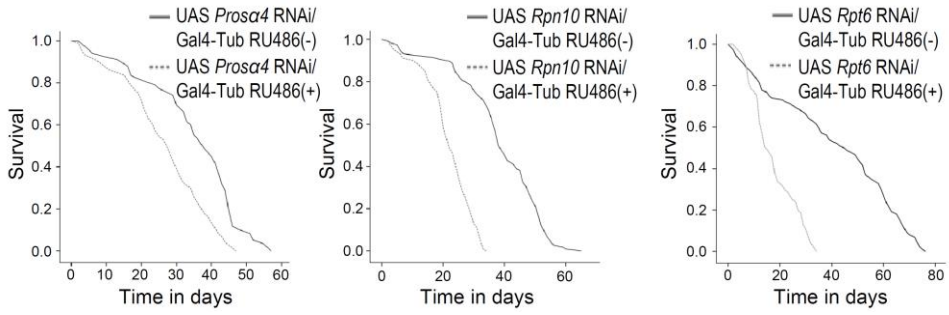

Figure S1. KD of the *Prosα4* (20S), *Rpn10* (19S) or *Rpt6* (19S) proteasomal genes reduces flies' longevity. Flies' longevity curves after inducible KD of the *Prosα4*, *Rpn10* or *Rpt6* genes. Statistics of the longevity curves are reported in Table S1.

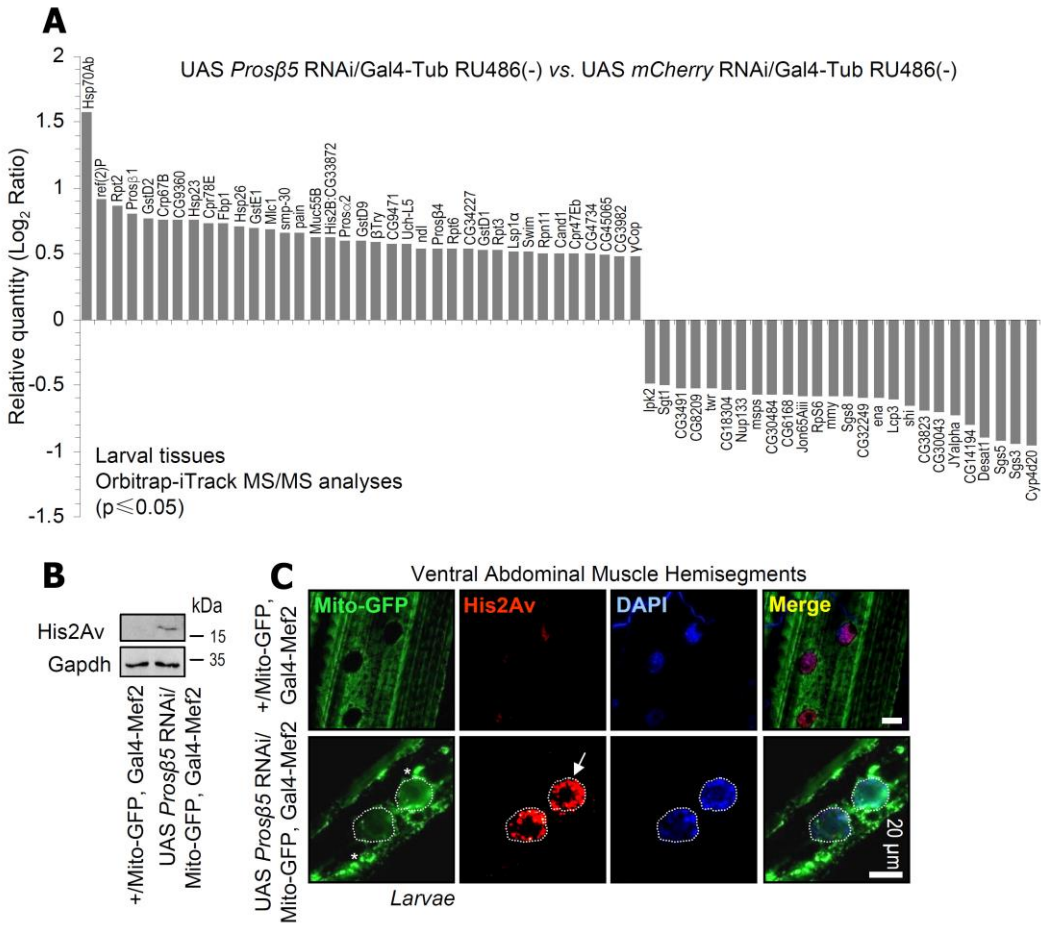

Figure S2. Proteomic analyses by nano-LC-ESI-MS/MS and His2Av stain in larvae tissues after KD of the 20S *Prosβ5* gene. (**A**) Graphical representation of the high resolution iTRAQ proteomics data. Proteins identified by iTRAQ proteomics to be differentially expressed (*vs*. *mCherry* RNAi) after inducible *Prosβ5* RNAi in larval tissues, along with their human orthologs, are reported in Table S2. Data refer to 3rd instar stage larvae not treated with RU486. (**B**) Immunoblot analyses after probing shown tissue lysates with His2Av antibody. (**C**) CLSM visualization of Mito-GFP reporter and of His2Av (immunofluorescence staining) in larvae muscle tissues of the shown genotypes; samples were counterstained with DAPI. White arrow indicates His2Av positive nuclei foci after *Prosβ5* KD; stars denote mitochondrial aggregates, some of which tend to be perinuclear. Gapdh probing (**B**) was used as input reference.

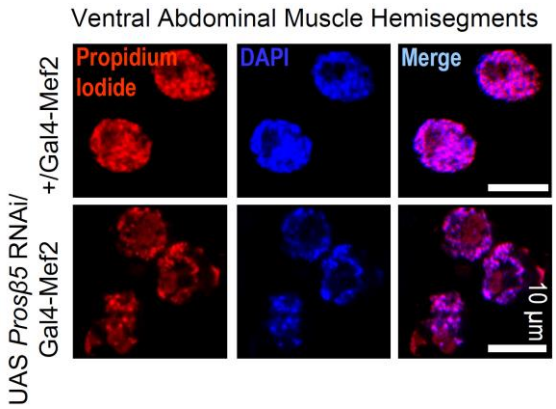

Figure S3. Proteasome KD induces DNA damage. CLSM visualization of propidium iodide and DAPI staining in muscle nuclei of 3rd instar stage larvae expressing the shown transgenes.

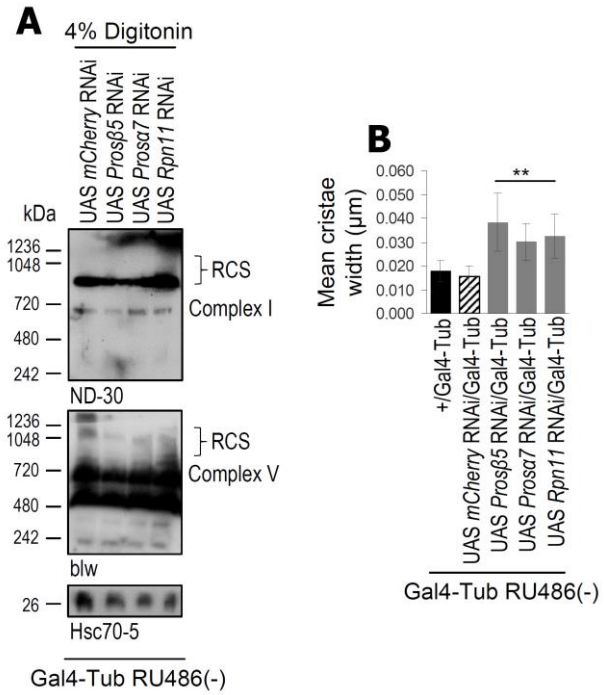

Figure S4. Disruption of mitochondrial functionality after proteasome KD. (**A**) Immunoblots after BN-PAGE (4% digitonin), for the analysis of mitochondrial RCS assembly, and probing with antibodies against ND-30/NDUFS3 (complex I) and blw/ATP5F1A (complex V); mitochondria were isolated from larvae tissues expressing *mCherry*, *Prosβ5*, *Prosα7* or *Rpn11* RNAi transgenes. (**B**) Mean mitochondrial cristae width in larvae of the shown genotypes. In both cases the Gal4-Tub driver was used. Bars, ± SD; n ≥2; $^{**}P < 0.01$.

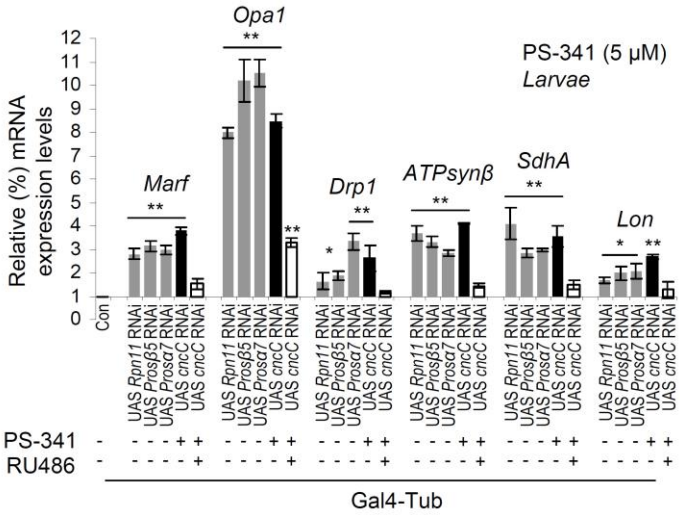

Figure S5. Proteasome dysfunction promotes a cncC-dependent induction of mitostatic genes. Relative expression of *Marf*, *Opa1*, *Drp1*, *ATPsynβ*, *SdhA* and *Lon* genes in 3rd instar stage control larvae or after KD of the shown proteasomal subunits (larvae were not exposed to RU486). Larvae were also treated with 5 µM of the proteasome inhibitor PS-341 in parallel (or not) to *cncC* KD (induced with RU486). Gene expression was plotted *vs*. the respective control set to 1; the *RpL32/rp49* gene expression was used as input reference. Bars, ± SD; n ≥2; **P* < 0.05; ***P* < 0.01.

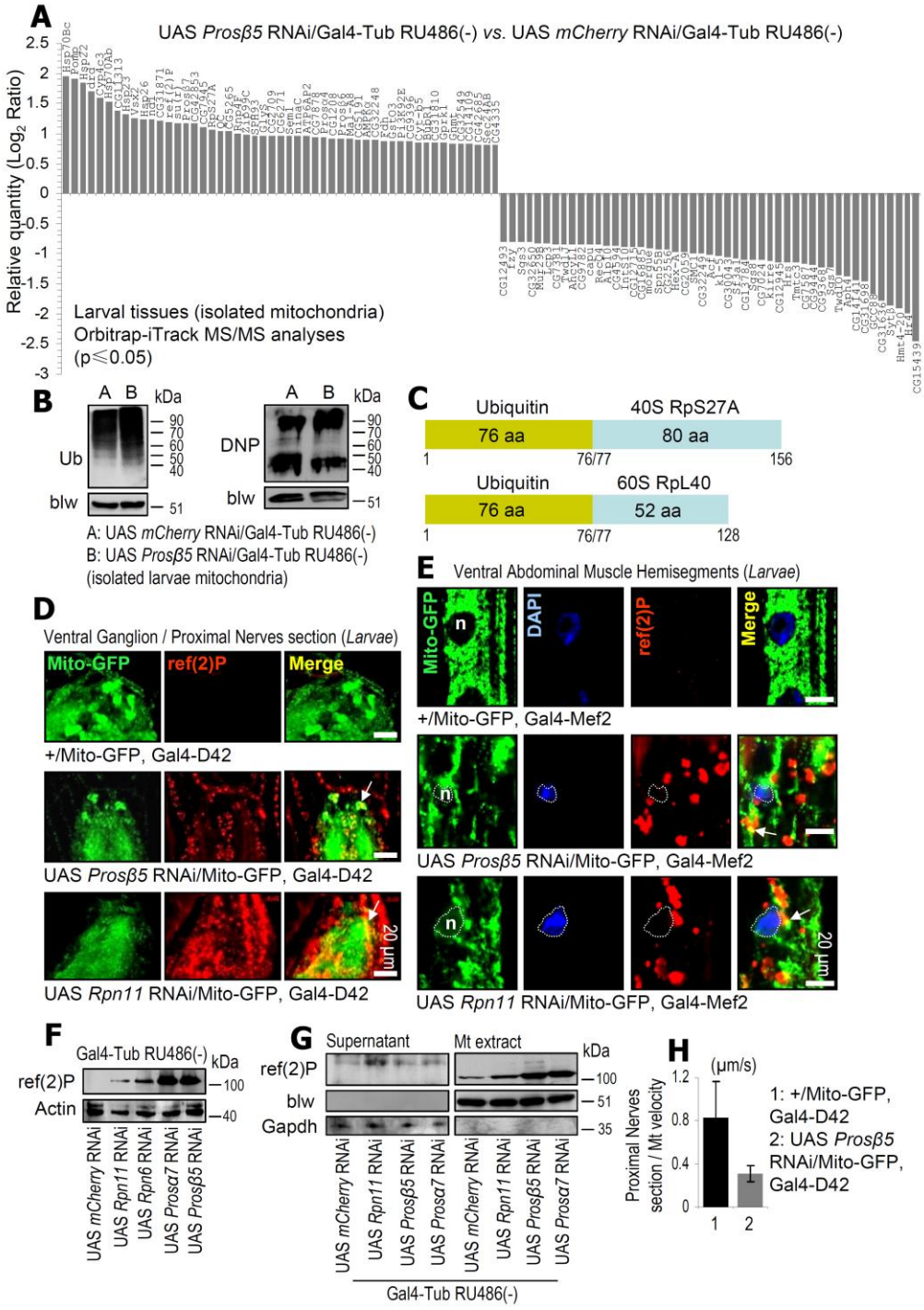

Figure S6. Proteomic analyses by nano-LC-ESI-MS/MS in purified mitochondria after KD of the 20S proteasomal *Prosβ5* subunit; and ref(2)P colocalization with mitochondria in the nervous system and muscle tissues after KD of proteasome subunits. (**A**) Graphical representation of the iTRAQ proteomics data. Proteins identified by iTRAQ proteomics to be differentially expressed (*vs*. *mCherry* RNAi) after inducible *Prosβ5* RNAi in isolated mitochondria from larval tissues, along with their human orthologs, are reported in Table S3. (**B**) Immunoblot analyses of isolated mitochondria of the shown larvae genotypes after probing samples with antibodies against ubiquitin (Ub; left panel) or protein carbonylation (DNP; right panel). (**C**) Graphical representation of the ribosomal 40S RpS27A

and 60S RpL40 proteins domains. (**D**) CLSM visualization of mitochondria (Mito-GFP reporter) in the nervous system of larvae after *Prosβ5* or *Rpn11* KD; tissues were also stained with ref(2)P antibody. (**E**) CLSM visualization of Mito-GFP and ref(2)P distribution in larvae muscle of the shown genotypes; samples were counterstained with DAPI (n, nucleus). (**F, G**) Immunoblot analyses showing ref(2)P expression levels in larvae tissues (**F**) or following mitochondria isolation (**G**). (**H**) Quantitative analysis of mitochondria velocity in larvae nervous tissue after *Prosβ5* KD (see also, Videos S1, S2). White arrows in (**D**, **E**) indicate ref(2)P colocalization with aggregated mitochondria. In (**A**, **B**, **F, G**) data refer to 3rd instar stage larvae not treated with RU486 (driver, Gal4-Tub). blw/ATP5F1A (**B**, **G**) and Actin (**F**) or Gapdh (**G**) probing were used as input reference.

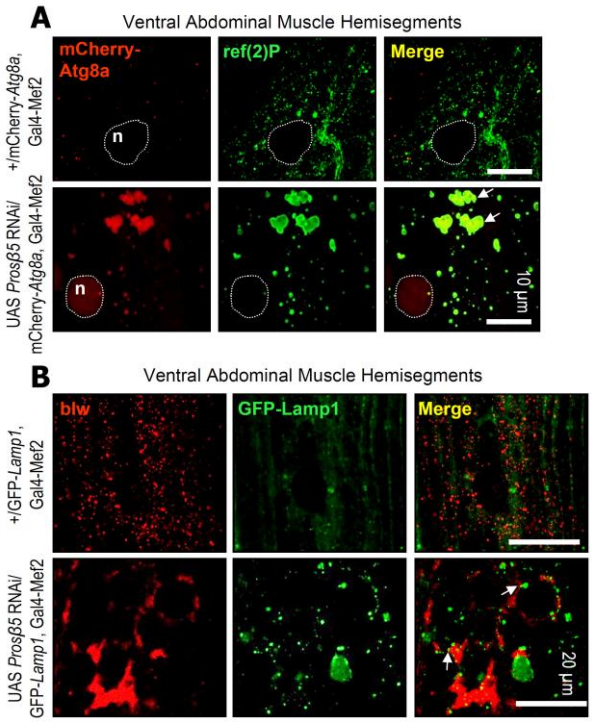

Figure S7. mCherry-Atg8a colocalization with ref(2)P, and blw/ATP5F1A with GFP-Lamp1 in larvae muscles following KD of the *Prosβ5* gene. (**A**) CLSM visualization of mCherry-Atg8a and ref(2)P costaining. (**B**) CLSM visualization of mitochondrial blw/ATP5F1A staining and GFP-Lamp1. White arrows in (**A**), (**B**) indicate sites of colocalization; n, nucleus.

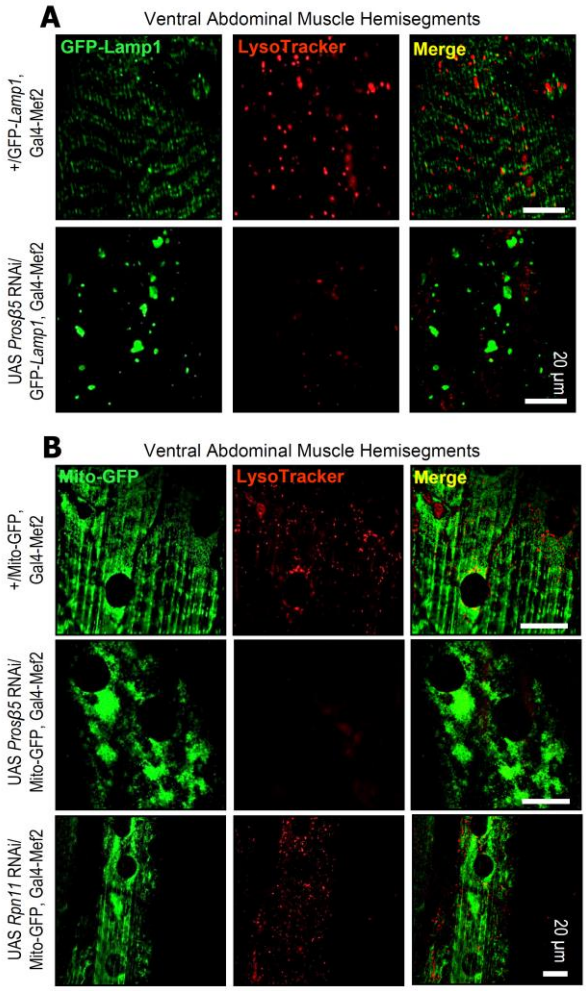

Figure S8. KD of the *Prosβ5* proteasomal gene induces GFP-Lamp1 in larval muscle but results in reduced LysoTracker Red staining; on the contrary, *Rpn11* KD increased LysoTracker Red staining. (**A**) CLSM visualization of GFP-Lamp1 signal and LysoTracker Red staining in control larvae or after KD of the *Prosβ5* gene. (**B**) CLSM visualization of Mito-GFP and LysoTracker Red in control larvae or after KD of the *Prosβ5* or the *Rpn11* genes.

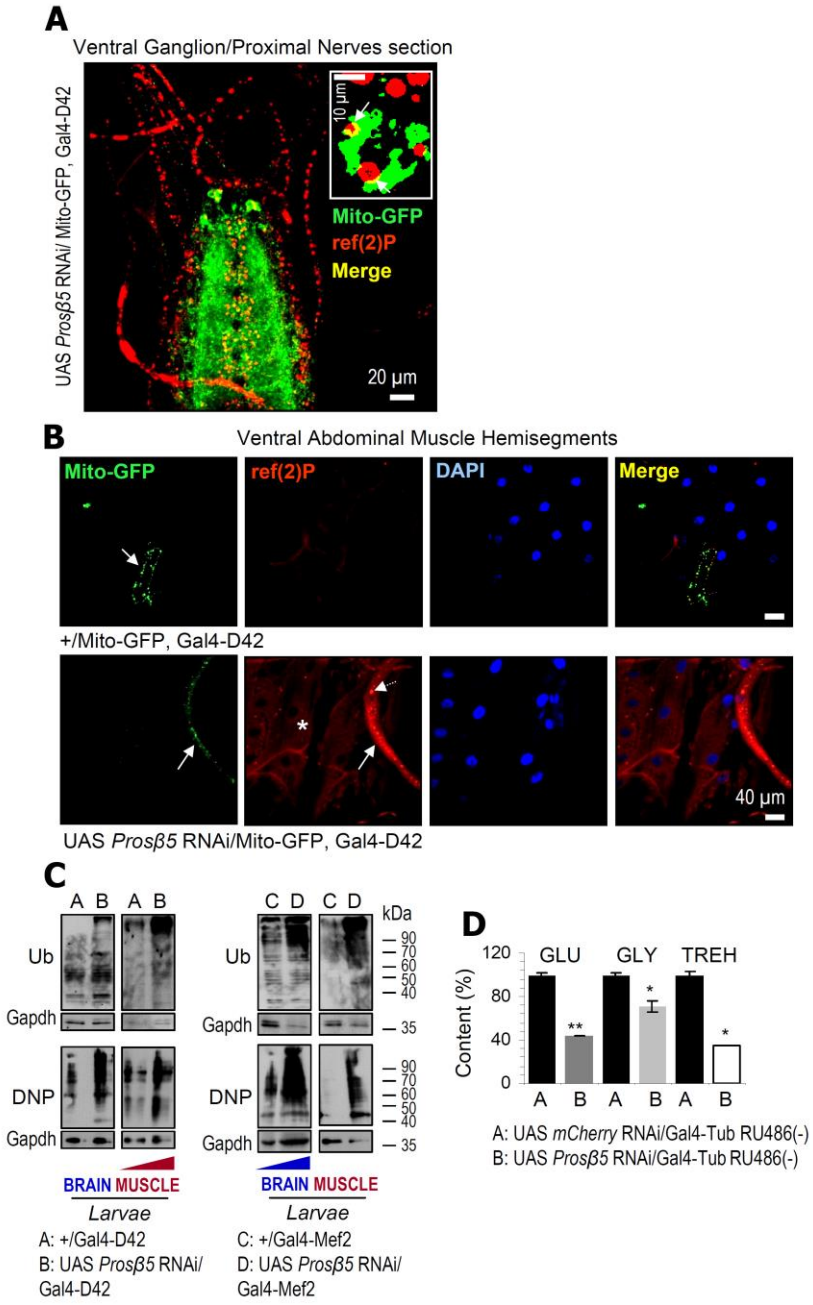

Figure S9. Targeted proteasome KD in the nervous system or muscles promotes systemic effects; ubiquitous proteasome KD in larvae induces metabolic alterations. (**A**, **B**) CLSM visualization of Mito-GFP and ref(2)P localization in larvae nervous system (**A**; shown Figure is an extended view of Fig. S6D, middle panel) and muscles (**B**) after targeted KD of the *Prosβ5* gene in the nervous system [in (**B**) samples were counterstained with DAPI]. Arrows in (**A**) indicate ref(2)P colocalization with aggregated mitochondria, while in (**B**) indicate nerves that express Mito-GFP; dashed arrow in (**B**) denotes ref(2)P staining in Mito-GFP positive nerves and white star ref(2)P staining in underlying muscles. (**C**) Immunoblot analyses, after KD of the *Prosβ5* proteasomal gene in the nervous system (Gal4-D42 driver) or in the muscles (Gal4-Mef2 driver) and probing of isolated brain or muscle samples with antibodies against protein ubiquitination (Ub) or carbonylation (DNP). (**D**) Relative (%) content (*vs*. controls) of GLU, GLY and TREH after *Prosβ5* KD in larvae tissues; data refer to 3rd

instar stage larvae not treated with RU486. Gapdh probing (**C**) was used as input reference. In (**D**) control values were set to 100%. Bars, ± SD; n ≥2; *$P < 0.05$; **$P < 0.01$.

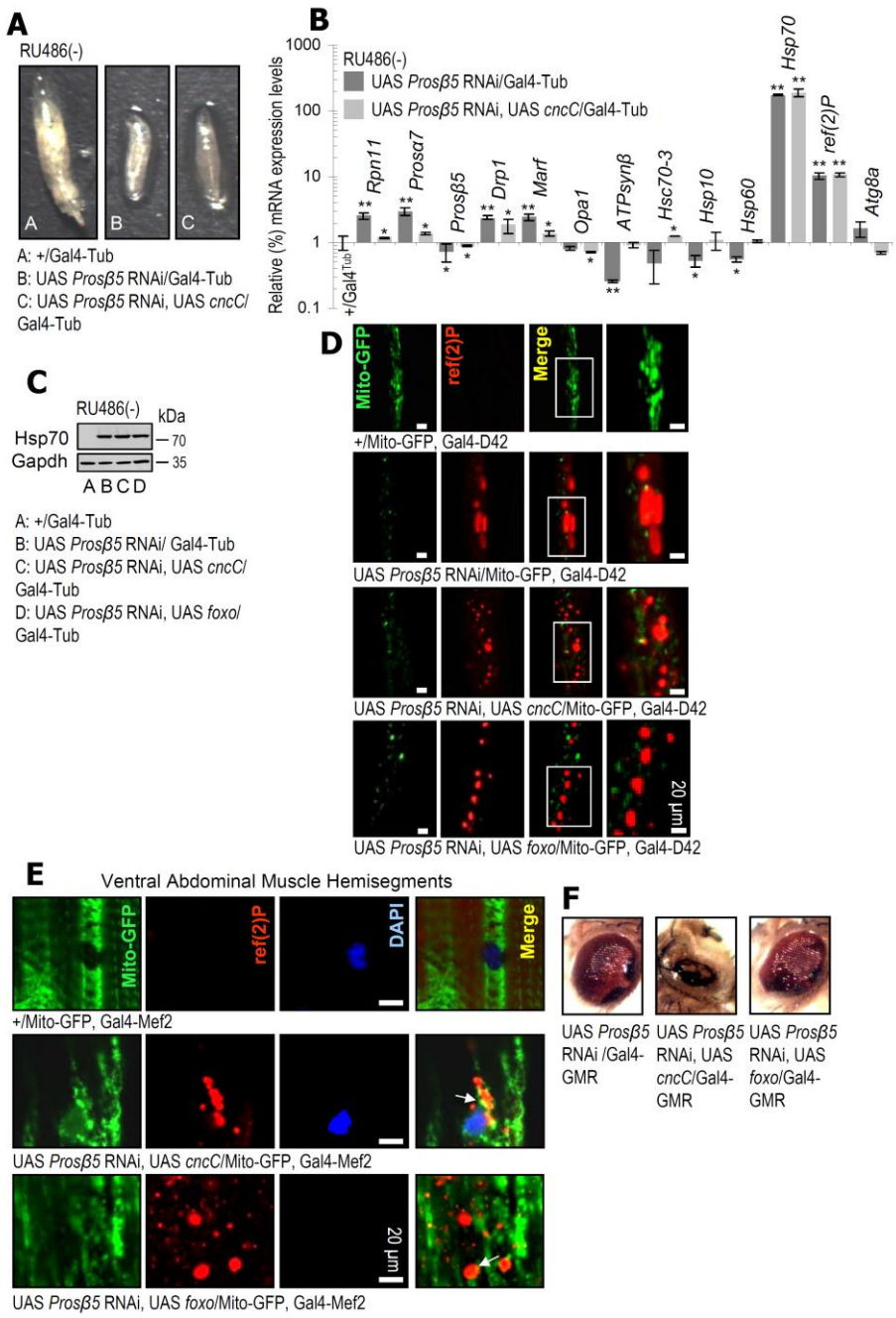

Figure S10. Higher *cncC* or *foxo* expression levels do not rescue the toxic effects of proteasome loss of function. (**A**) Stereoscope viewing of 3rd instar control (+/Gal4-Tub) or transgenic larvae expressing the indicated transgenes. (**B**) Relative expression of *Rpn11*, *Prosα7*, *Prosβ5*, *Drp1*, *Marf*, *Opa1*, *ATPsynβ*, *Hsc70-3*, *Hsp10*, *Hsp60*, *Hsp70*, *ref(2)P* and *Atg8α* genes in control samples, after *Prosβ5* KD or after combined *Prosβ5* KD and *cncC* OE. (**C**) Immunoblotting analyses of protein samples from shown transgenic larvae tissues; samples were probed with antibodies Hsp70 and Gapdh. (**D, E**) CLSM visualization of the Mito-GFP reporter in the nervous system (**D**) or in muscle tissues (**E**) of the shown transgenic larvae; samples were stained with a ref(2)P antibody and in (**E**) were also counterstained with DAPI. (**F**) Stereoscope viewing of flies' eyes after targeted eye expression of the indicated transgenes; for control adult flies' eyes (+/Gal4-GMR) see Fig. 4B. Unless otherwise

indicated, data refer to 3rd instar stage larvae not exposed to RU486 (driver, Gal4-Tub). Gene expression was plotted *vs*. the respective control set to 1. Right panels in (**D**) represent increased magnification (white rectangles) from merged CLSM images. White arrows in (**E**) indicate ref(2)P colocalization with aggregated mitochondria. Gapdh (**C**) and *RpL32/rp49* gene (**B**) probing were used as input reference. Bars, ± SD; n ≥2; **P* < 0.05; ***P* < 0.01.

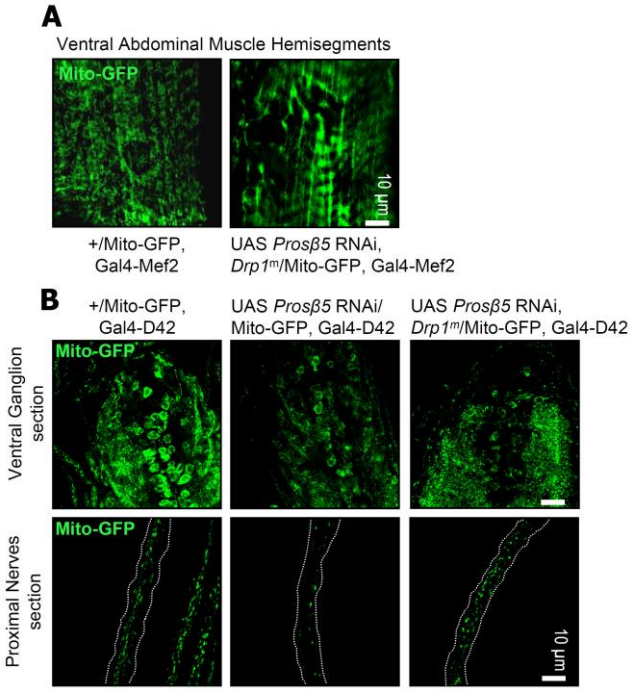

Figure S11. Mitochondria visualization in muscle and nervous tissues following KD of the *Prosβ5* gene and *Drp1*^{m} expression. CLSM visualization of mitochondria (Mito-GFP reporter) in larval muscles (**A**) and nervous (**B**) tissues; dashed lines denote proximal nerves section.

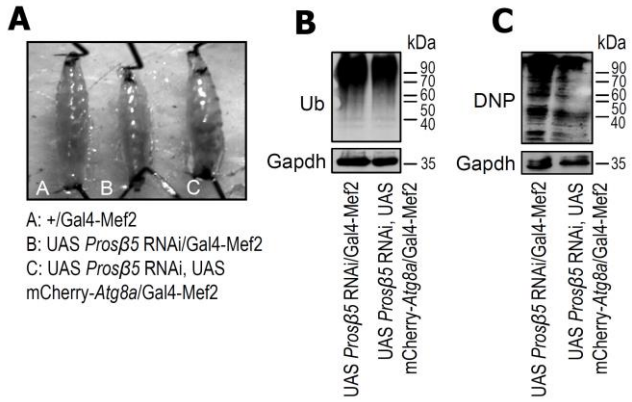

Figure S12. Enhanced *Atg8a* expression alleviates proteasome dysfunction-induced proteome instability. (**A**) Stereoscope viewing of 3rd instar control (+/Gal4-Mef2) or transgenic larvae expressing the shown transgenes in muscles (Gal4-Mef2 driver). (**B**, **C**) Immunoblotting analyses of tissue protein samples from shown transgenic larvae; samples were probed with antibodies against ubiquitinated (Ub) (**B**) and carbonylated (DNP) (**C**) proteins. Gapdh probing was used as input reference.

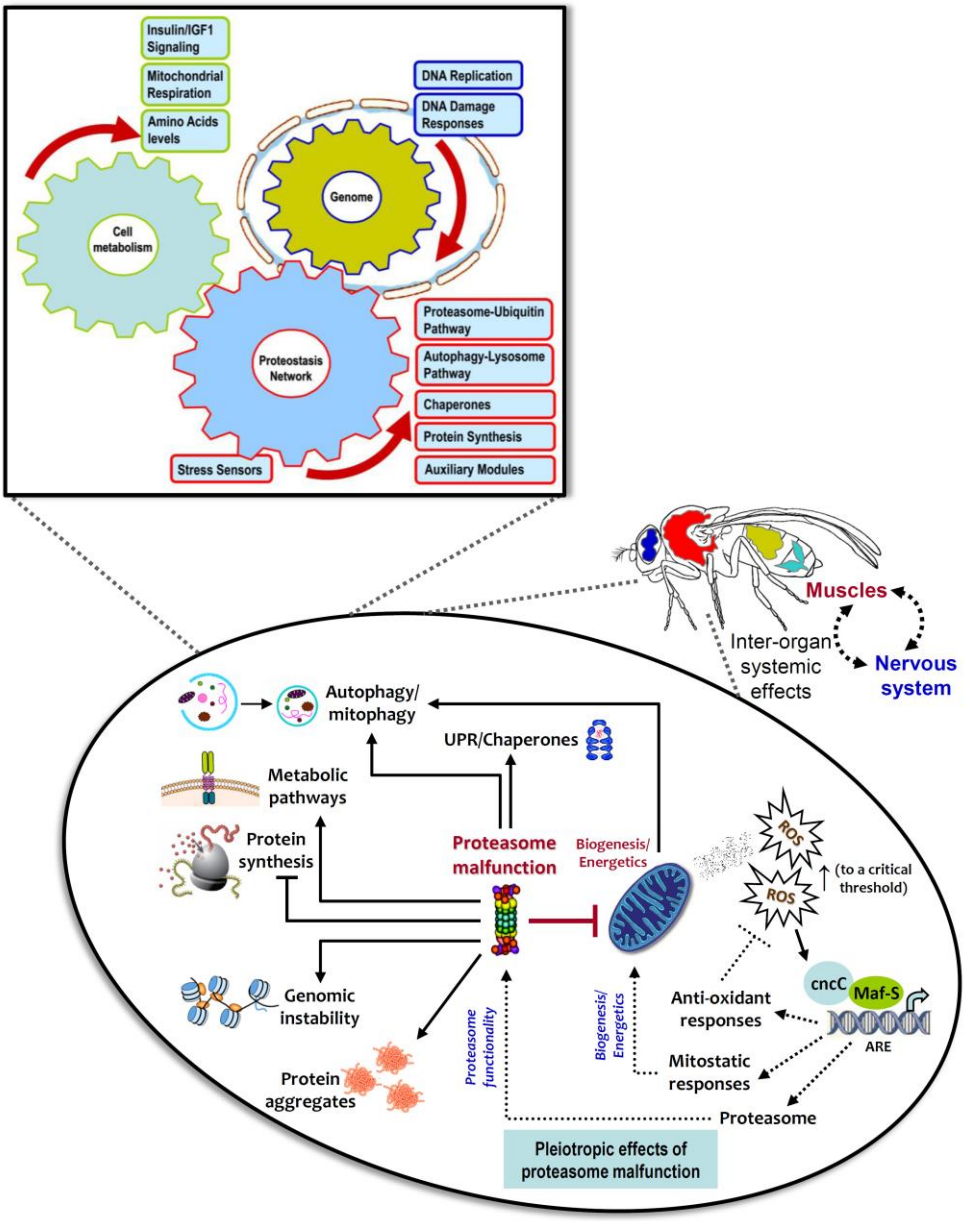

Figure S13. Our findings indicate that proteasome is a central hub in the wiring of proteostatic, mitostatic, nutrients sensing and likely genome maintenance modules. Therefore, loss of proteasome functionality results in increased genomic instability, as well as in deregulation of proteostatic and mitostatic networks affecting thus all machineries that maintain cellular homeodynamics and energetics.

Supplemental Tables

Table S1. Summary of lifespan experiments.

Table S2. Proteins found to be differentially expressed after inducible *Prosβ5* RNAi (*vs*. *mCherry* RNAi) in larval tissues (nano-LC-ESI-MS/MS proteomics analysis).

Table S3. Proteins found to be differentially expressed after inducible *Prosβ5* RNAi (*vs*. *mCherry* RNAi) in isolated mitochondria from larval tissues (nano-LC-ESI-MS/MS proteomics analysis).

Table S4. Proteins found to be increasingly ubiquitinated in larvae mitochondria after inducible *Prosβ5* RNAi (*vs*. *mCherry* RNAi) (nano-LC-ESI-MS/MS proteomics analysis).

Supplemental Videos

Video S1. Mitochondrial motility in the nervous system (proximal nerves section) of control larvae (~20 s; representative video).

Video S2. Mitochondrial motility in the nervous system (proximal nerves section) after targeted *Prosβ5* RNAi in larvae nervous system (~20 s; representative video).

KEY RESOURCES TABLES

REAGENT OR RESOURCE	SOURCE	IDENTIFIER
Chemicals, Peptides		
Tris-HCl	Applichem	A3452
$MgCl_2$	Sigma-Aldrich	13152
ATP	Sigma-Aldrich	1905
DTT	Applichem	A2948
Glycerol	Applichem	A2926
Boric acid	Applichem	A2940
Trizma base	Sigma-Aldrich	T1503
Acrylamide	Sigma-Aldrich	A3574
TEMED	Applichem	A1148
Ammonium persulfate	Applichem	A1142

Sucrose	Applichem	A2211
BSA	Sigma-Aldrich	A9418
EDTA	Applichem	A2937
5% Digitonin	Thermo Fisher Scientific	BN2006
KH_2PO_4	Applichem	A1043
Hepes	Biosera	PM-B2093
Glutamic acid	Sigma-Aldrich	G1251
Diethyl malate	Sigma-Aldrich	W237418
Oligomycin	Sigma-Aldrich	75351
FCCP	Cayman Chemical	370-86-5
EGTA	Applichem	A0878
Triton X-100	Applichem	A4975
Paraformaldehyde	Scharlau	PA00950500
Glutaraldehyde	Applichem	A0589
Sodium cacodylate	Sigma-Aldrich	G0250
OsO_4	Sigma-Aldrich	75632
Epon	Sigma-Aldrich	45345
Formic acid	Sigma-Aldrich	251364
Acetonitrile	Sigma-Aldrich	271004
$CHCl_3$	Sigma-Aldrich	439142
MeOH	Scharlau	ME0316005l
Na_2HPO_4	Sigma-Aldrich	S3264
NaN_3	Applichem	A1430
KCl	Applichem	131494
$CDCl_3$	Applichem	133101

Chloroquine	Sigma-Aldrich	C6628
RU486	Sigma-Aldrich	M8046
Protein-A Sepharose beads	GE Healthcare	17-0974-01
Suc-Leu-Leu-Val-Tyr-AMC-LLVY	Enzo Life Sciences	BML-P802-0005
Z-Leu-Leu-Glu-AMC-LLE	Enzo Life Sciences	BML-ZW9345-0005
Boc-Leu-Arg-Arg-AMC-LRR	Enzo Life Sciences	BML-BW8515-0005
z-FR-AMC	Enzo Life Sciences	BML-P139-0050
NativePAGE™ 5% G-250 Sample Additive	Thermo Fisher Scientific	BN2004
Amyloglucosidase	Sigma-Aldrich	A7420
Trehalase	Sigma-Aldrich	T8778
Critical Commercial Assays/Kits		
Bradford assay	Bio-Rad	5000006
OxyBlot	Millipore	#s7150
iTRAQ kit	ABSciex	4381662
Native sample buffer	Invitrogen™	BN20032
GLU Reagent	Sigma-Aldrich	GAGO-20
Mowiol®	Sigma-Aldrich	4-88
Genomic DNA Kit	Thermo Fisher Scientific	#K0512
DreamTaq Green PCR Master Mix	Thermo Fisher Scientific	#K1082
Maxima First Strand cDNA Synthesis Kit	Thermo Fisher Scientific	#K1642
SYBR Green/ROX qPCR Master Mix	Thermo Fisher Scientific	#K0223
Nitrocellulose membrane	Macherey-Nagel GmbH	741280
PVDF membrane	Macherey-Nagel GmbH	741290

Fluorescent dyes		
Propidium Iodide	BioLegend	421301
Oligonucleotides		
See Method Details for primer sequences	This study	N/A
Software and Algorithms		
MS Excel	Microsoft	N/A
IBM SPSS; version 19.0	IBM	N/A
ImageJ	Wayne Rasband (NIH)	N/A
Digital Eclipse Nikon C1 software	Nikon Inc.	N/A
INGENUITY® PATHWAY ANALYSIS	QIAGEN Bioinformatics	N/A
ICON-NMR v. 4.2.6.	Bruker Biospin	N/A
AMIX Statistics v. 3.9.14	Bruker Biospin	N/A
SIMCA-P+ v. 11.5	Umetrics AB, Sweden	N/A

CONTACT FOR REAGENT AND RESOURCE SHARING

Further information and requests for reagents may be directed to Ioannis Trougakos (itrougakos@biol.uoa.gr).

Supplemental Materials and Methods

Genes list.

Atg6 (Autophagy-related 6, FBgn0264325, CG5429); *Atg8a* (Autophagy-related 8a, FBgn0052672, CG32672); *ATPsynβ* (ATP synthase, β subunit, FBgn0010217, CG11154); *blw* (bellwether, FBgn0011211, CG3612); *cncC* (cap-n-collar isoform-C, FBgn0262975, CG43286); *Drp1* (Dynamin related protein 1, FBgn0026479, CG3210); *foxo* (forkhead box, sub-group O, FBgn0038197, CG3143); *fzo* (fuzzy onions, FBgn0011596, CG4568); *His2Av* (Histone H2A variant, FBgn0001197, CG5499); *Hsf* (Heat shock factor, FBgn0001222, CG5748); *Hsp23* (Heat shock protein 23, FBgn0001224, CG4463); *Hsp2*6 (Heat shock protein 26, FBgn0001225, CG4183); *Hsp70* (Heat-shock-protein-70Bb/a, FBgn0013278/FBgn0013277, CG31359/CG31449); *Keap1* (Keap1, FBgn0038475, CG3962); *Lon* (Lon protease, FBgn0036892, CG8798); *Marf* (Mitochondrial assembly

regulatory factor, FBgn0029870, CG3869); *ND-30* [NADH dehydrogenase (ubiquinone) 30 kDa subunit, FBgn0266582, CG12079)]; *Opa1* (Optic atrophy 1, FBgn0261276, CG8479); *park* (parkin, FBgn0041100, CG10523); *Pink1* (PTEN-induced putative kinase 1, FBgn0029891, CG4523); *Prosα4* (Proteasome α4 subunit, FBgn0004066, CG3422); *Prosα7* (Proteasome α7 subunit, FBgn0023175, CG1519); *Prosβ1* (Proteasome β1 subunit, FBgn0010590, CG8392); *Prosβ2* (Proteasome β2 subunit, FBgn0023174, CG3329); *Prosβ5* (Proteasome β5 subunit, FBgn0029134, CG12323); *ref(2)P* (refractory to sigma P, FBgn0003231, CG10360); *RpL40* (Ribosomal protein L40, FBgn0003941, CG2960); *Rpn6* (Regulatory particle non-ATPase 6, FBgn0028689, CG10149); *Rpn10* (Regulatory particle non-ATPase 10, FBgn0015283, CG7619); *Rpn11* (Regulatory particle non-ATPase 11, FBgn0028694, CG18174); *RpS27A* (Ribosomal protein S27A, FBgn0003942, CG5271); *Rpt6* (Regulatory particle triple-A ATPase 6, FBgn0020369, CG1489); *SdhA* (Succinate dehydrogenase, subunit A (flavoprotein), FBgn0261439, CG17246); *Trxr-1* (Thioredoxin reductase-1, FBgn0020653, CG2151).

Genomic DNA Extraction and PCR analysis.

For checking lines carrying more than one transgene, genomic DNA from flies or larvae was extracted with a Genomic DNA Kit (Thermo Fisher Scientific, K0512). In brief, flies or larvae were homogenized in lysis buffer and the homogenate was incubated for 10 min at 65°C. Chloroform was added and after centrifugation the aqueous phase was collected. DNA was then precipitated with the addition of 1X precipitation buffer. PCR analysis was performed by using the DreamTaq Green PCR Master Mix (Thermo Fisher Scientific, K1082) and PCR products were visualized by agarose gel electrophoresis.

Primers (F: Forward; R: Reverse) sequences were as follows: *Valium 20*-F: ACCAGCAACCAAGTAAATCAAC, *Valium 20*-R: TAATCGTGTGTGATGCCTACC; *cncC*-F: TGGAATTGGGCACCCATGGCG, *cncC*-R: AGTTTGAGTACGTCGTTCAACA; *foxo*-F: CAGTGCCGGATGGAAGAACT, *foxo*-R: ATCCACCAGGATGACTTGCC; *Marf*-F: CCGCTATCCCGGTTCAACTC, *Marf*-R: ACCTTCATGTGATCCCGCTG; *Marf* RNAi-F: CGCGAATTCCCGAGGGCTTTCAGATACGCTACTTC, *SV40*-R: CACAGAAGTAAGGTTCCTTCACAAAGATCC; *Atg8α* -F: ACGCCTTCGAGAAGCGTCGC, *Atg8α*-R: CCAAATCACCGATGCGCGCC; *Opa1*-F: CGAGGAGTTCCTACTTGC, *Opa1*-R: TGAGATTCCGCGAGAACTGG.

Larval brain isolations for immunoblotting.

For larval brain isolation third instar larvae were collected and dissected in PBS into a Petri anatomy dish. Larvae were immobilized with 2 small pins (1 to the top and 1 to the edge of larvae) so that the abdominal region was upwards; cut just above the edge and then a slit was made into the larvae mouth to enable removal of the internal organs and the isolation of the intact brain.

Propidium iodide staining.

For propidium iodide staining fixed larvae tissues were incubated with 400 μg/ml RNAse A (Thermo Fisher Scientific, EN0531) for 40 min in PBS containing 0.3% Triton X-100 (Applichem, A4975), washed 3X with PBS containing 0.3% Triton X-100 and incubated with propidium iodide (500 ng/ml; BioLegend, 421301) for 20 min. Following 3 washes with PBS (Applichem, A9201 PB), samples were mounted in Mowiol® 4-88 (Sigma-Aldrich, 4-88) and viewed in CLSM.

CLSM recording of mitochondria motility in Drosophila Larval Neurons.

To image mitochondria in live segmental nerves, larvae were prepared as described before [1] with minor modifications. Third instar larvae were dissected in Schneider's insect medium (Thermo Fisher Scientific, 21720024). The space between the glass and the coverslip glass was filled with Schneider's insect medium. To track the mitochondria movement, GFP mitochondria were visualized with a Digital Eclipse C1 Nikon CLSM at 25°C. Mitochondria in the proximal segment (A2) and middle segment (A4) of the axons were observed. A 55-μm region of the segmental nerve was photobleached for 15 s with 488 nm light at full intensity from the Digital Eclipse C1 Nikon CLSM (60x objective, zoom factor 4). Immediately after photobleaching, images were collected at a rate of 1 frame/s (zoom factor 2.5) for 280 s. To track and quantify mitochondria movement the NIH ImageJ version 1.62b7 was used with an object tracking macro (MTrackJ) based on software designed by Erik Meijering.

Measurement of GLU, TREH and GLY levels.

GLU, TREH and GLY levels were performed as described previously [2] with minor modifications. Larvae tissues were homogenized in cold PBS for GLU and GLY measurements or with trehalase buffer (5 mM Tris, pH 6.6, 137 mM NaCl, 2.7 mM KCl) for TREH measurement. The clear extract was then incubated for 10 min at 70ºC and a small amount was used for protein quantification by Bradford assay. Following centrifugation at max speed for 3 min, 30 μl of diluted (1/4) (or undiluted for TREH measurement) supernatant was transferred to a 96-well plate. The GLU assay was performed by adding in the sample 100 μl of GLU Reagent (Sigma-Aldrich, GAGO-20) and incubating for 30 min at 37ºC. For GLY measurement the same procedure as the GLU assay was followed except that the samples were incubated with or without 1 U of amyloglucosidase (Sigma-Aldrich, A7420). For TREH measurement 100 μl of the GLU Reagent (Sigma-Aldrich, GAGO-20) were added in the samples which were then incubated for 18 hours at 37ºC; followed by incubation (or not) with 0.05 U/ml of trehalase (Sigma-Aldrich, T8778). Absorbance was recorded at 540 nm and the TREH or GLY levels were calculated after the substraction of the GLU measurement at this step from the total amount of free GLU measured after TREH or amyloglucosidase digestion. At least 3 replicates per genotype or experimental condition were performed.

Sample preparation and nano-LC-ESI-MS/MS analysis of iTRAQ labeled peptides.

Larvae tissues or isolated mitochondria were homogenized with the dissolution buffer (0.5 M triethylammonium bicarbonate) from the iTRAQ kit (ABSciex, 4381663), mixed with vortex and after the addition of 0.05% SDS were sonicated (20% power with 0.1-0.2 pulses) for 20 s on ice. Homogenates were centrifuged for 15 min at 13,000 × g (4ºC); supernatant was collected and protein content was measured with the Bradford assay. Recovered protein (50 µg) was diluted in dissolution buffer (solution C) up to a final volume of 20 µl, followed by the addition of 2 µl reducing reagent from the iTRAQ kit; samples were then incubated for 1 h at 60ºC. Following the addition of 1 µl cysteine blocking reagent [200 mM methyl methanethiosulfonate (Sigma-Aldrich, 208795) in isopropanol] from the iTRAQ kit, samples were incubated for 10 min at room temperature (RT). Proteins were digested with overnight incubation (at RT in dark) after the addition of 75 ng/µl trypsin (protein:trypsin, 30:1) and were subsequently labeled with the iTRAQ reagents as per manufacturer's instructions.

LC-MS experiments were performed on a Dionex Ultimate 3000 UHPLC system coupled with the high resolution nano-ESI Orbitrap-Elite mass spectrometer (Thermo Fisher Scientific, 168 3rd Avenue. Waltham, MA USA 02451). Individual high-pH RP peptide fractions were reconstituted in 50 µl loading solution composed of 0.1% formic acid. A 5-µl volume was injected and loaded on the Acclaim PepMap 100, 100 µm × 2 cm C18, 5 µm, 100 Å trapping column with the ulPickUp Injection mode; the loading pump was operating at flow rate of 5 µl/min. For the peptide separation, the Acclaim PepMap RSLC, 75 µm × 50 cm, nanoViper, C18, 2 µm, 100 Å column retrofitted to a PicoTip emitter was used for multi-step gradient elution. Mobile phase (A) was composed of 0.1% formic acid and mobile phase (B) was composed of 100% acetonitrile, 0.1% formic acid. The peptides were eluted under a 315 minute gradient from 2% (B) to 33% (B). Flow rate was 300 nl/min and column temperature was set at 35°C. Gaseous phase transition of the separated peptides was achieved with positive ion electrospray ionization applying a voltage of 2.5 kV. For every MS survey scan, the top 10 most abundant multiply charged precursor ions between m/z ratio 300 and 2200 and intensity threshold 500 counts were selected with FT mass resolution of 60,000 and subjected to HCD fragmentation. Tandem mass spectra were acquired with FT resolution of 15,000. Normalized collision energy was set to 33 and already targeted precursors were dynamically excluded for further isolation and activation for 45 s with 5 ppm mass tolerance.

Supplemental References

1. Pilling AD, Horiuchi D, Lively CM, et al. Kinesin-1 and Dynein are the primary motors for fast transport of mitochondria in *Drosophila* motor axons. Mol Biol Cell. 2006;17:2057-2068.
2. Barrio L, Dekanty A, Milán M. MicroRNA-mediated regulation of Dp53 in the *Drosophila* fat body contributes to metabolic adaptation to nutrient deprivation. Cell Rep. 2014;8:528-541.

Table S1. Summary of lifespan experiments.

Figure	Sample	Mean Lifespan (LF) +/- s.e.m. (Days)		Median Lifespan +/- s.e.m. (Days)		% Median LF *vs*. control	Max (Days)	Log Rank P Value		
								UAS *Prosα4* RNAi/Gal4-Tub RU486 (-)	UAS *Prosα4* RNAi/Gal4-Tub RU486 (+)	*Total Animals Died/Tota*
Fig. S1	UAS *Prosα4* RNAi/Gal4-Tub RU486 (-)	35.128	1.665	38	2.835	100	57		0.000	62/70
	UAS *Prosα4* RNAi/Gal4-Tub RU486 (+)	26.587	1.293	28	1.967	73.68	47	0.000		79/87
								UAS *Rpn10* RNAi/Gal4-Tub RU486 (-)	UAS *Rpn10* RNAi/Gal4-Tub RU486 (+)	*Total Animals Died/Tota*
Fig. S1	UAS *Rpn10* RNAi/Gal4-Tub RU486 (-)	38.266	1.279	39	1.374	100	65		0.000	111/117
	UAS *Rpn10* RNAi/Gal4-Tub RU486 (+)	21.832	0.774	22	1.116	56.41	34	0.000		101/101
								UAS *Rpt6* RNAi/Gal4-Tub RU486 (-)	UAS *Rpt6* RNAi/Gal4-Tub RU486 (+)	*Total Animals Died/Tota*
Fig. S1	UAS *Rpt6* RNAi/Gal4-Tub RU486 (-)	41.086	2.253	45	5.083	100	76		0.000	98/117
	UAS *Rpt6* RNAi/Gal4-Tub RU486 (+)	17.495	0.859	15	1.256	33.33	34	0.000		101/101
								UAS *Rpt6* RNAi/Gal4-Tub RU486 (+)	UAS *Rpt6* RNAi, UAS *Opa1*/Gal4-Tub RU486 (+)	UAS *Rpt6* RNAi, *Drp1*^{m}/Gal4-Tub RU486 (+)	*Total Animals Died/Total*
Fig. 5D	UAS *Rpt6* RNAi/Gal4-Tub RU486 (+)	20.240	0.495	21	0.415	100	24		0.000	0.000	57/60
	UAS *Rpt6* RNAi, UAS *Opa1*/Gal4-Tub RU486 (+)	27.865	0.758	27	1.864	128.57	36	0.000		0.110	82/82
	UAS *Rpt6* RNAi, *Drp1*^{m}/Gal4-Tub RU486 (+)	27.489	1.113	30	1.659	142.85	37	0.000	0.110		75/77
								UAS *Rpt6* RNAi/Gal4-Tub RU486 (+)	UAS *Rpt6* RNAi, UAS *GFP-Atg8a*/Gal4-Tub RU486 (+) line 1	UAS *Rpt6* RNAi, UAS *GFP-Atg8a*/Gal4-Tub RU486 (+) line 2	*Total Animals Died/Tota*
Fig. 7C	UAS *Rpt6* RNAi/Gal4-Tub RU486 (+)	19.021	0.571	19	0.751	100	29		0.000	0.000	91/91
	UAS *Rpt6* RNAi, UAS *GFP-Atg8a*/Gal4-Tub RU486 (+) line 1	22.556	0.616	22	0.636	115.78	37	0.000		0.167	88/88
	UAS *Rpt6* RNAi, UAS *GFP-Atg8a*/Gal4-Tub RU486 (+) line 2	23.580	0.930	21	1.640	110.52	39	0.000	0.167		62/62

Table S2. Proteins found to be differentially expressed after inducible *Prosβ5* RNAi (*vs*. *mCherry* RNAi) in larval tissues (nano-LC-ESI-MS/MS proteomics analysis).

Uniprot_Acc	Fly GeneID	FlyBaseID	Fly Symbol	UAS *Prosβ5* RNAi (-) *vs.* UAS *mCherry* RNAi	UAS *Prosβ5* RNAi (-) *vs.* UAS *mCherry* RNAi L2R_p.values	Biological Process (UniProt)
P02825	44920	FBgn0013276	Hsp70Ab	1.57337414	1.32822E-10	Response to heat / Protein folding
P14199	35246	FBgn0003231	ref(2)P	0.91958927	0.000173634	Mitochondrion organization / Ub-dependent catabolism
P48601	42828	FBgn0015282	Rpt2	0.86888129	0.000388843	Proteasome subunit
A0AQH0	46058	FBgn0010590	Prosβ1	0.808694993	0.000960636	Proteasome subunit
Q9VG98	48335	FBgn0010038	GstD2	0.769370251	0.001682283	glutathione peroxidase activity
Q9VSY0	39081	FBgn0035985	Crp67B	0.76086192	0.001893089	Structural constituent of chitin-based larval cuticle
Q9VYU9	32128	FBgn0030332	CG9360	0.753923045	0.002082684	Oxidoreductase activity
P02516	39077	FBgn0001224	Hsp23	0.751837889	0.002142972	Response to heat / Protein folding
Q9VP00	40408	FBgn0037114	Cpr78E	0.735193682	0.002684668	Structural constituent of chitin-based larval cuticle
Q04691	39566	FBgn0000639	Fbp1	0.730345962	0.002864483	Storage protein import into fat body
P02517	39075	FBgn0001225	Hsp26	0.713120878	0.003595938	Response to heat / Protein folding
Q7KK90	37106	FBgn0034335	GstE1	0.696314779	0.004469485	Glutathione transferase activity
P06742	43323	FBgn0002772	Mlc1	0.686397569	0.005071101	Microfilament motor activity
Q9VFG5	41786	FBgn0038257	smp-30	0.656931517	0.007314502	Cold acclimation / Negative regulation of imaginal disc-derived wing size
Q9W0Y6	37985	FBgn0060296	pain	0.655698363	0.00742534	Involved in detection of pain sensation due to high temperature
A1ZB24	37057	FBgn0034294	Muc55B	0.626502265	0.010529528	Extracellular matrix structural constituent
P02283	3771809	FBgn0053872	His2B:CG33872	0.622131901	0.011082302	Core component of nucleosome
P40301	41531	FBgn0086134	Prosα2	0.605663221	0.013403919	Proteasome subunit
Q9VGA0	41502	FBgn0038020	GstD9	0.59482267	0.015157559	Glutathione transferase activity
P35004	47901	FBgn0010357	βTry	0.59336674	0.015407844	Cleavage: Arg-|-Xaa, Lys-|-Xaa
Q9VH72	41197	FBgn0037749	CG9471	0.575474471	0.018793796	NADPH dehydrogenase activity
Q9XZ61	39102	FBgn0011327	Uch-L5	0.575464061	0.018795942	Ubiquitin carboxyl-terminal hydrolase
P98159	38738	FBgn0002926	ndl	0.543264515	0.026548937	serine-type endopeptidase activity / dorsal-ventral pathway of the embryo
Q9VJJ0	34999	FBgn0032596	Prosβ4	0.543019184	0.026617296	Proteasome subunit
O18413	33105	FBgn0020369	Rpt6	0.542765448	0.026688157	Proteasome subunit
A1Z8H0	36186	FBgn0085256	CG34227	0.533675164	0.029336552	
P20432	41503	FBgn0001149	GstD1	0.526144641	0.031698824	Glutathione transferase activity
Q9V405	32047	FBgn0028686	Rpt3	0.522827507	0.032790058	Proteasome subunit
P11995	32199	FBgn0002562	Lsp1α	0.518201215	0.034365573	Larval storage protein; may serve as a store of amino acids for synthesis of adult proteins
Q7JWQ7	37537	FBgn0034709	Swim	0.515598665	0.035279994	Positive regulation of Wnt signaling pathway
Q9V3H2	33738	FBgn0028694	Rpn11	0.504527225	0.03940556	Proteasome subunit
Q9VKY2	34403	FBgn0027568	Cand1	0.503750143	0.039709911	Assembly factor of SCF (SKP1-CUL1-F-box protein) E3 ubiquitin ligase complexes
Q7K0A2	36189	FBgn0033598	Cpr47Eb	0.499495968	0.041411665	Structural constituent of chitin-based larval cuticle
A1Z9B8	36477	FBgn0033826	CG4734	0.49828757	0.041906166	
Q8MQY9	19835504	FBgn0266435	CG45065	0.488921384	0.0459111	Ecdysteroid metabolic process
Q9VSY3	39084	FBgn0035988	CG3982	0.48463476	0.0478489	
Q8I0G5	43717	FBgn0028968	γCOP	0.482763124	0.048716298	Coatomer subunit
Q9VPR6	33236	FBgn0031267	Ipk2	-0.48525005	0.047566597	Inositol-1,4,5-trisphosphate 3-kinase activity
Q9VHT3	40982	FBgn0265101	Sgt1	-0.496540245	0.042630039	Protein binding, bridging
Q9V453	34870	FBgn0028887	CG3491	-0.522314428	0.032961685	Regulation of transcription, DNA-templated
Q9VSC5	38888	FBgn0035830	CG8209	-0.526576118	0.031559196	Nucleic acid binding
O97066	40815	FBgn0262801	twr	-0.526576118	0.031559196	Cleavage of hydrophobic, N-terminal signal or leader sequences from secreted and periplasmic proteins
M9NCS3	33969	FBgn0031869	CG18304	-0.537646826	0.028152833	
Q9VCW3	42680	FBgn0039004	Nup133	-0.539524983	0.027607551	Probable component of the nuclear pore complex
E1JIM4	41952	FBgn0027948	msps	-0.567447858	0.020513306	
A1Z9I2	36534	FBgn0050484	CG30484	-0.569228713	0.020120387	
Q9VTH7	39273	FBgn0036154	CG6168	-0.575502806	0.018787957	Metalloendopeptidase activity
Q9VRS7	38683	FBgn0035665	Jon65Aiii	-0.57760183	0.018359751	Srerine-type endopeptidase activity
Q95TP9	31700	FBgn0261592	RpS6	-0.581291288	0.017627771	Structural constituent of ribosome
Q8IPJ6	33903	FBgn0259749	mmy	-0.582972991	0.017302699	UDP-N-acetylglucosamine diphosphorylase activity
P02842	39285	FBgn0003378	Sgs8	-0.586439398	0.016649192	Extracellular matrix structural constituent
Q8IRB2	317939	FBgn0052249	CG32249	-0.600195594	0.014264627	
Q8T4F7	37201	FBgn0000578	ena	-0.600195594	0.014264627	Functions, together with Abl, trio and fra, in a complex signaling network that regulates axon guidance at the CNS midline
P07188	35819	FBgn0002534	Lcp3	-0.612348736	0.012414094	Component of the larval cuticle
P27619	45928	FBgn0003392	shi	-0.651024338	0.00785925	Shibire mutation is the cause of temperature-sensitive paralysis
Q9W408	31573	FBgn0029863	CG3823	-0.691580305	0.004748127	Transporter activity
Q8MKL0	246412	FBgn0050043	CG30043	-0.701171047	0.004199147	
A8QI34	5740846	FBgn0267363	JYalpha	-0.723088283	0.003154304	Sodium:potassium-exchanging ATPase activity
M9PHY0	32908	FBgn0030996	CG14194	-0.805033671	0.001013113	
Q7K4Y0	117369	FBgn0086687	Desat1	-0.901352002	0.000233127	Cuticle hydrocarbon biosynthetic process
P07701	42114	FBgn0003375	Sgs5	-0.91481816	0.000187643	Extracellular matrix structural constituent
P02840	39288	FBgn0003373	Sgs3	-0.947737793	0.000109057	Extracellular matrix structural constituent
Q9W011	38311	FBgn0035344	Cyp4d20	-0.953018876	9.98046E-05	Involved in the metabolism of insect hormones and in the breakdown of synthetic insecticides

Table S3. Proteins found to be differentially expressed after inducible *Prosβ5* RNAi (*vs*. *mCherry* RNAi) in isolated mitochondria from larval tissues (nano-LC-ESI-MS/MS proteomics analysis).

Uniprot_Acc	Fly GeneID	FlyBaseID	Fly Symbol	UAS *Prosβ5* RNAi (-) *vs.* UAS *mCherry* RNAi	UAS *Prosβ5* RNAi (-) *vs.* UAS *mCherry* RNAi L2R_p.values	Biological Process (UniProt)
Q8INI8	48583	FBgn0013279	Hsp70Bc	1.95177271	2.13664E-06	Response to heat / Protein folding
Q9VIJ5	35342	FBgn0032884	Pomp	1.905805565	3.68473E-06	Proteasome assembly
P02515	3772576	FBgn0001223	Hsp22	1.842320058	7.66849E-06	Chaperone-mediated protein folding
Q8IR42	318102	FBgn0260006	drd	1.697435018	3.74994E-05	Cuticle development
Q9VA27	43663	FBgn0015032	Cyp4c3	1.600825878	0.000101179	Metabolism of insect hormones / breakdown of synthetic insecticide
P02825	44920	FBgn0013276	Hsp70Ab	1.524526906	0.000213529	Response to heat
Q9VA44	43646	FBgn0039798	CG11313	1.379136495	0.000810002	Hemolymph coagulation/proteolysis
P02516	39077	FBgn0001224	Hsp23	1.305221099	0.001525207	Chaperone-mediated protein folding
Q9W4B3	31469	FBgn0263512	Vsx2	1.258759197	0.002235588	Development / transcription factor activity
P02517	39075	FBgn0001225	Hsp26	1.239844391	0.002603279	Chaperone-mediated protein folding
P98159	38738	FBgn0002926	ndl	1.2335048	0.002738383	Peptidase / dorsal-ventral axis specification
Q9VKS5	34463	FBgn0051871	CG31871	1.203241015	0.003475944	Lipase activity
P14199	35246	FBgn0003231	ref(2)P	1.193696631	0.003743583	Mitochondrion organization / Ub-dependent catabolism
Q9W374	31858	FBgn0086450	su(r)	1.167374695	0.004581535	Pyrimidine base degradation
Q9VNA5	40639	FBgn0250746	Prosβ7	1.166983676	0.004595173	Proteasome subunit
C0PDE0	10178880	FBgn0262100	CG42853	1.16007435	0.004842286	
Q95RY2	39679	FBgn0036505	CG7945	1.101030919	0.007496355	Protein folding
P15357	34420	FBgn0003942	RpS27A	1.053977056	0.010476982	Ubiquitin-40S ribosomal protein S27A
Q9VRQ9	38663	FBgn0052412	QC	1.050289433	0.010750059	Glutaminyl-peptide cyclotransferase activity
Q9VEM4	42074	FBgn0038486	CG5265	1.033052661	0.012112176	Carnitine O-acetyltransferase activity
Q9W4D2	31448	FBgn0014024	Rnp4F	0.990437334	0.016156359	RNA processing / central nervous system development
Q9VAF0	43533	FBgn0039714	Zip99C	0.975089278	0.017880185	Iron ion transmembrane transporter activity
Q9VJD7	35049	FBgn0032638	SPH93	0.965178885	0.019077059	Peptidase activity
Q9VFC8	41823	FBgn0266064	GlyS	0.957953039	0.019993323	Glycogen (starch) synthase activity
O76908	31264	FBgn0024977	CG2709	0.954691672	0.020419306	Formation of DNA double-strand breaks during meiosis
Q9VB88	43252	FBgn0039476	CG6271	0.950433395	0.020987402	Lipid catabolic process
Q9VM46	50428	FBgn0266666	Sem1	0.949501363	0.021113566	Proteasome assembly
P10676	34012	FBgn0002938	ninaC	0.947271784	0.021418054	Putative serine/threonine-protein kinase and myosin activities
Q9VHG4	41104	FBgn0037671	ATP6AP2	0.947247745	0.021421358	Frizzled binding
Q7K4L8	40959	FBgn0037549	CG7878	0.940530527	0.022362068	RNA secondary structure unwinding
P22769	32584	FBgn0004066	Prosα4	0.930171812	0.023883136	Proteasome subunit
A8JQU1	40727	FBgn0037386	CG1208	0.914607506	0.026337099	Glucose transmembrane transporter activity
P40304	39855	FBgn0002284	Prosβ6	0.912465	0.026691403	Proteasome subunit
A1Z7F3	35830	FBgn0033297	Mal-A8	0.903420643	0.028232791	Alpha-1,4-glucosidase activity
Q7KSA4	42431	FBgn0038803	CG5191	0.894084558	0.029903749	Glutaminyl-tRNA synthase (glutamine-hydrolyzing) activity
O18645	43904	FBgn0023169	AMPKα	0.889993224	0.030662389	AMP-activated protein kinase activity
Q8IRB1	317938	FBgn0052248	CG32248	0.885970072	0.031424443	
P46415	41311	FBgn0011768	Fdh	0.880790881	0.032429347	Catalyzes the oxidation of long-chain primary alcohols and the oxidation of S-(hydroxymethyl) glutathione
Q9VSL2	38972	FBgn0035904	GstO3	0.878491945	0.03288415	Glutathione transferase activity
P91634	42446	FBgn0015279	Pi3K92E	0.87473702	0.033638738	1-phosphatidylinositol-3-kinase activity / Autophagy
Q9VHB2	41156	FBgn0037714	CG9396	0.872288838	0.034138658	Mitochondrial pyruvate transmembrane transport
Q9V4N3	35688	FBgn0264294	Cyt-b5	0.849001197	0.039219731	Electron carrier for several membrane-bound oxygenases
A1Z6I7	35522	FBgn0263855	BubR1	0.848330278	0.03937516	Meiosis sister chromatid cohesion / Positive regulation of chromatin silencing
Q8SX47	318955	FBgn0051810	CG31810	0.844383634	0.040300082	Integral component of membrane
P32865	3355013	FBgn0260798	Gprk1	0.839995335	0.041350077	Phosphorylates the activated forms of G protein-coupled receptors
Q9VG42	41561	FBgn0038074	Gnmt	0.822297625	0.045822788	Glycine N-methyltransferase activity / Response to starvation
Q7KUW2	32822	FBgn0052549	CG32549	0.820315336	0.046348253	5'-nucleotidase activity

Q9VU75	39512	FBgn0036364	CG14109	0.818722068	0.046774266	
Q9VJS0	34854	FBgn0261571	CG42685	0.818162552	0.046924651	
A1Z813	36025	FBgn0033460	Sec24AB	0.817386208	0.047133987	Cargo loading into COPII-coated vesicle
Q9VDM7	42421	FBgn0038795	CG4335	0.813303318	0.048247885	Carnitine biosynthetic process
M9PHF9	38575	FBgn0035571	CG12493	-0.808118356	0.049694247	Double-stranded RNA binding
Q24044	34968	FBgn0001086	fzy	-0.808137326	0.049688889	Anaphase-promoting complex binding / Ubiquitin protein ligase activity
P02840	39288	FBgn0003373	Sgs3	-0.808571823	0.049566316	Extracellular matrix structural constituent
Q9VYI7	326227	FBgn0052650	CG32650	-0.810206808	0.049107351	
Q8IPF8	319014	FBgn0051901	Mur29B	-0.811126886	0.048850643	Extracellular matrix structural constituent
P07188	35819	FBgn0002534	Lcp3	-0.817062978	0.047221376	Structural constituent of chitin-based larval cuticle
Q8MSQ3	41589	FBgn0038098	CG7381	-0.832573885	0.043178537	
Q9VBD6	43206	FBgn0039440	TwdlJ	-0.835137235	0.042539414	Structural constituent of chitin-based cuticle
Q9VZX9	38342	FBgn0035371	AhcyL1	-0.836995785	0.04208104	Involved in step 1 of the subpathway that synthesizes L-homocysteine from S-adenosyl-L-homocystein
Q9VXE4	32632	FBgn0030763	CG9782	-0.837505391	0.041956088	
B7Z014	33611	FBgn0000256	capu	-0.847755833	0.039508654	Microtubule binding / Actin nucleation
Q9VSE6	53438	FBgn0040290	RecQ4	-0.848658957	0.039298951	DNA helicase activity / Base-excision repair
Q9VRM8	38632	FBgn0035619	Alp10	-0.853025691	0.038298293	Alkaline phosphatase activity
Q9VL67	34316	FBgn0032161	CG4594	-0.86311663	0.03606848	Fatty acid beta-oxidation
Q9VZM7	38444	FBgn0035462	IntS10	-0.881548652	0.032280621	Small nuclear RNAs processing
Q9VYH4	32252	FBgn0030443	CG12715	-0.888456279	0.030951619	
Q8SZM2	34811	FBgn0032538	CG16885	-0.891405593	0.030398652	
Q9Y165	33648	FBgn0027609	morgue	-0.896691383	0.029428839	K48-linked polyubiquitin binding
Q7JV69	49803	FBgn0028983	Spn55B	-0.921011234	0.025302244	Negative regulation of proteolysis / Serine-type endopeptidase inhibitor activity
Q9VYM2	32201	FBgn0030396	CG2556	-0.926435832	0.024453336	
Q9GNH8	45875	FBgn0001186	Hex-A	-0.959883856	0.019744803	Cellular glucose homeostasis / Glycolysis
Q9W3R8	31663	FBgn0029942	CG2059	-0.973712101	0.018042469	Carboxylic ester hydrolase activity
Q9VCD8	42853	FBgn0040283	SMC1	-0.983591188	0.01690637	DNA repair / Mitotic sister chromatid cohesion
Q8IRB2	317939	FBgn0052249	CG32249	-0.999740657	0.0151841	
Q9V9T4	43751	FBgn0027620	Acf	-1.018930511	0.013339955	Chromatin assembly
Q5LJN5	3355175	FBgn0001315	kl-5	-1.038584631	0.01165922	Male fertility / Microtubule-based movement
Q8MKL0	246412	FBgn0050043	CG30043	-1.055075037	0.010396875	
Q9VEP9	42048	FBgn0266917	Sf3a1	-1.07230775	0.009209072	mRNA splicing, via spliceosome
M9PEZ6	34003	FBgn0031897	CG13784	-1.093134813	0.007936157	
P02842	39285	FBgn0003378	Sgs8	-1.103160003	0.007381571	Extracellular matrix structural constituent
Q9W4H4	31407	FBgn0029722	CG7024	-1.103347028	0.007371564	Catalyzes the overall conversion of pyruvate to acetyl-CoA and CO2
Q9W4T9	31292	FBgn0028369	kirre	-1.127147813	0.006193118	Cell adhesion molecule binding
Q9VH65	41204	FBgn0037755	CG12945	-1.132223169	0.005964922	
Q960X8	33458	FBgn0031450	Hrs	-1.137358689	0.00574176	Endosome membrane invagination and formation of multivesicular bodies / Early embryonic signalling pathways
Q7K4B6	37401	FBgn0020312	Tmtc3	-1.13813321	0.005708765	
Q9VEI6	42113	FBgn0038523	CG7587	-1.16512255	0.004660587	
Q9VH93	41175	FBgn0037730	CG9444	-1.184613112	0.004015557	Transporter activity
Q8MYU6	40135	FBgn0036890	CG9368	-1.220891652	0.003026409	
P02841	47198	FBgn0003377	Sgs7	-1.226403556	0.002897303	Extracellular matrix structural constituent
Q9VBD8	43204	FBgn0039438	TwdlO	-1.340782673	0.001129108	Structural constituent of chitin-based cuticle
Q24238	43671	FBgn0016123	Alp4	-1.362191914	0.000938968	Alkaline phosphatase activity
Q8SX06	39264	FBgn0036146	CG14141	-1.441499101	0.000463851	
Q8MS99	318888	FBgn0051698	CG31698	-1.458772888	0.000395966	
Q9VGR1	41350	FBgn0037881	GCC88	-1.670495186	4.97189E-05	Golgi vesicle transport
Q8IPJ5	318865	FBgn0051636	CG31636	-1.769556918	1.72716E-05	Transporter activity
Q9VUJ3	39630	FBgn0261090	Sytβ	-1.85408797	6.70591E-06	Calcium ion-dependent exocytosis
Q9W5E0	31015	FBgn0025639	Hmt4-20	-1.894551866	4.20294E-06	Trimethylates 'Lys-20' of histone H4
M9PDJ5	31162	FBgn0264562	Hr4	-1.993954477	1.2822E-06	Transcription, DNA-templated
Q9VQZ8	33651	FBgn0031606	CG15439	-2.450349443	2.6669E-09	Lateral inhibition

Table S4. Proteins found to be increasingly ubiquitinated* in larvae mitochondria after inducible *Prosβ5* RNAi (*vs*. *mCherry* RNAi) (nano-LC-ESI-MS/MS proteomics analysis).

Uniprot_Acc	MW [kDa]	calc. pI	Fly GeneID	FlyBaseID	Fly Symbol	Biological Process (UniProt)
H9BVD2	26.3	7.65			Polyubiquitin	Polyubiquitin
H9BVD3	26.3	8.69			Polyubiquitin	Polyubiquitin
H9BVD4	26.3	8.69			Polyubiquitin	Polyubiquitin
H9BVD5	26.3	7.65			Polyubiquitin	Polyubiquitin
H9BVD7	26.3	7.68			Polyubiquitin	Polyubiquitin
I7DFE1	20.0	10.15			Transposase	DNA integration
P0CG69	85.7	7.66	38456	FBgn0003943	Ubi-p63E	Polyubiquitin
P15357	17.9	9.77	34420	FBgn0003942	RpS27A	Ubiquitin-40S ribosomal protein S27a
P18101	14.7	9.83	33629	FBgn0003941	RpL40	Ubiquitin-60S ribosomal protein L40
Q24575	8.5	7.25			Ubi-p63E	*D. melanogaster* ubiquitin
Q24576	8.4	8.50			Ubi-p63E	*D. melanogaster* ubiquitin
Q24577	8.5	7.25			Ubi-p63E	*D. melanogaster* ubiquitin
Q7JPZ2	8.5	9.19			Ubi-p63E	*D. melanogaster* ubiquitin
Q7JPZ3	8.6	7.25			Ubi-p63E	*D. melanogaster* ubiquitin
Q8MSM5	119.9	7.71			Ubi-p63E	Protein Ubiquitination
Q8MT02	34.4	7.53			Ubi-p5E	Protein Ubiquitination
Q95ST9	76.5	7.94			SD09360p	
Q9VWN9	223.5	7.12	50356	FBgn0085430	CG34401	
Q9W418	60.0	7.62	326237	FBgn0086558	Ubi-p5E	Protein Ubiquitination
R9PY16	34.3	8.24	31564	FBgn0029856	CG11700	Adult lifespan, negative regulaiton of reproduction
R9PY27	223.3	7.17	50356	FBgn0085430	CG34401	

* Label free quantification following Ub-IP in purified mitochondrial preparations to identify over-ubiquitinated targets